Electronic Supplementary Material (ESI) for Journal of Materials Chemistry A.

Zwitterionic versus organic ionic plastic crystal electrolytes with mixed anions: probing the unique physicochemical and electrolyte properties

Faezeh Makhlooghiazad, Luke A. O'Dell, Jennifer M. Pringle

Supplementary Information

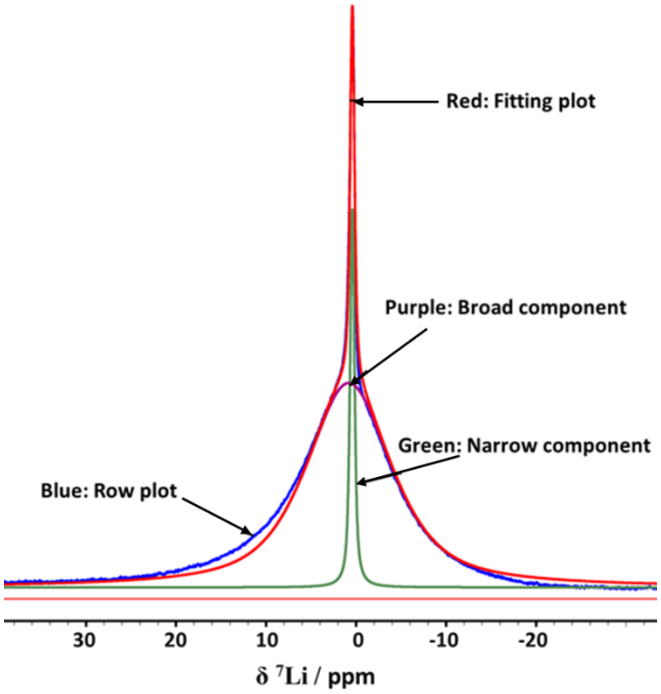

Figure S1. A fitting example of ^{7}Li NMR for 90 mol% $LiBF_4$ in ZI at 30 °C.

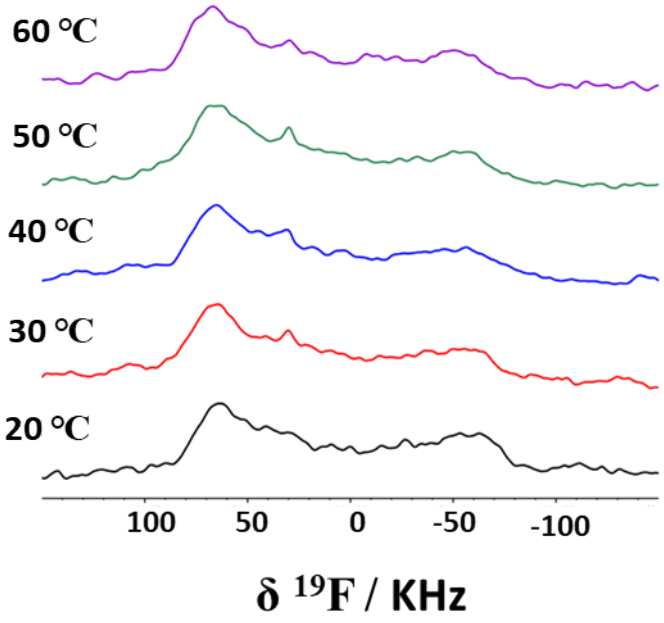

Figure S2. ^{19}F single-pulse spectra versus temperature of LiFSI

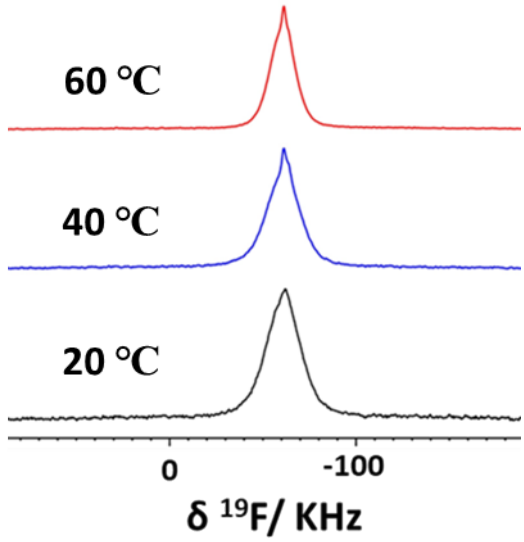

Figure S3. ^{19}F single-pulse spectra versus temperature of the neat ZI

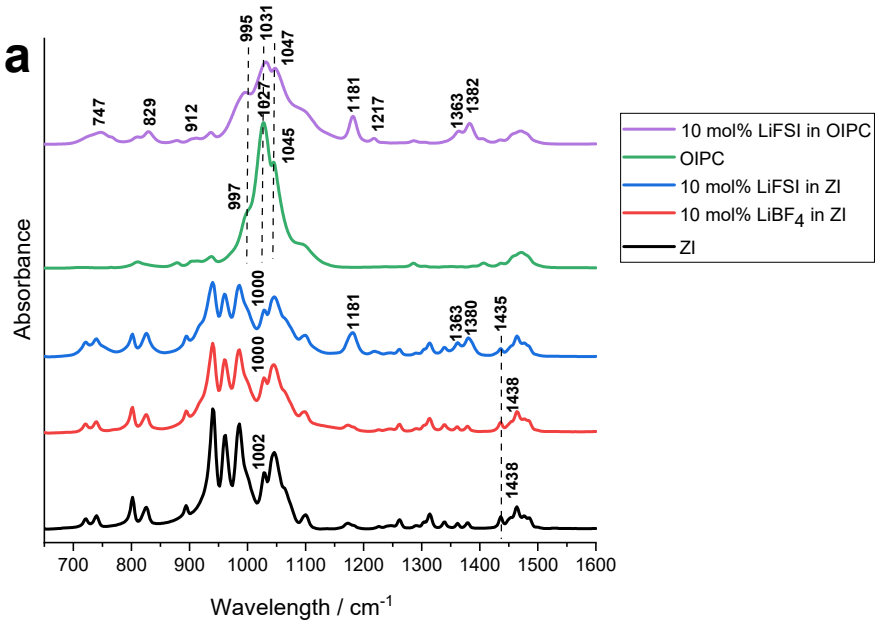
a
747
829
912
995
1031
1027
1047
1045
997
1181
1217
1363
1382
1000
1380
1435
1438
1002
Absorbance
700
800
900
1000
1100
1200
1300
1400
1500
1600
Wavelength / cm-1
10 mol% LiFSI in OIPC
OIPC
10 mol% LiFSI in ZI
10 mol% LiBF4 in ZI
ZI

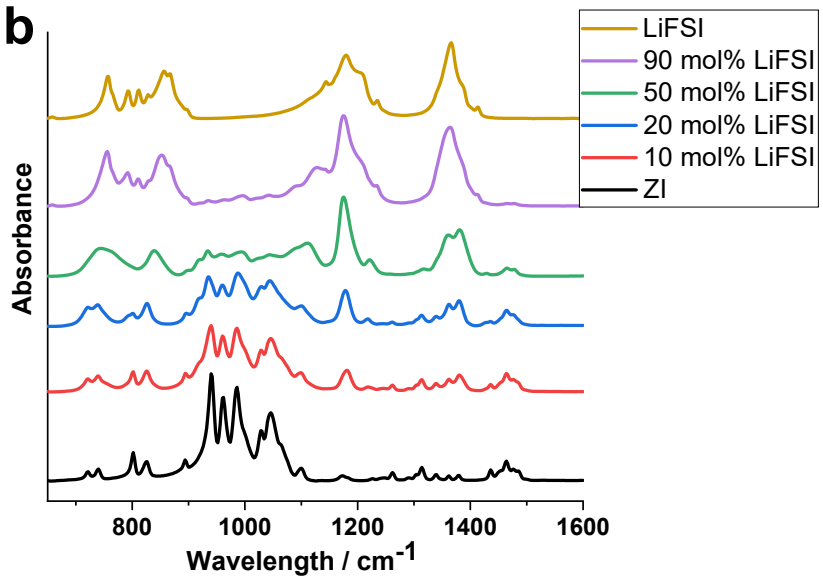
b
Absorbance
800
1000
1200
1400
1600
Wavelength / cm-1
LiFSI
90 mol% LiFSI
50 mol% LiFSI
20 mol% LiFSI
10 mol% LiFSI
ZI

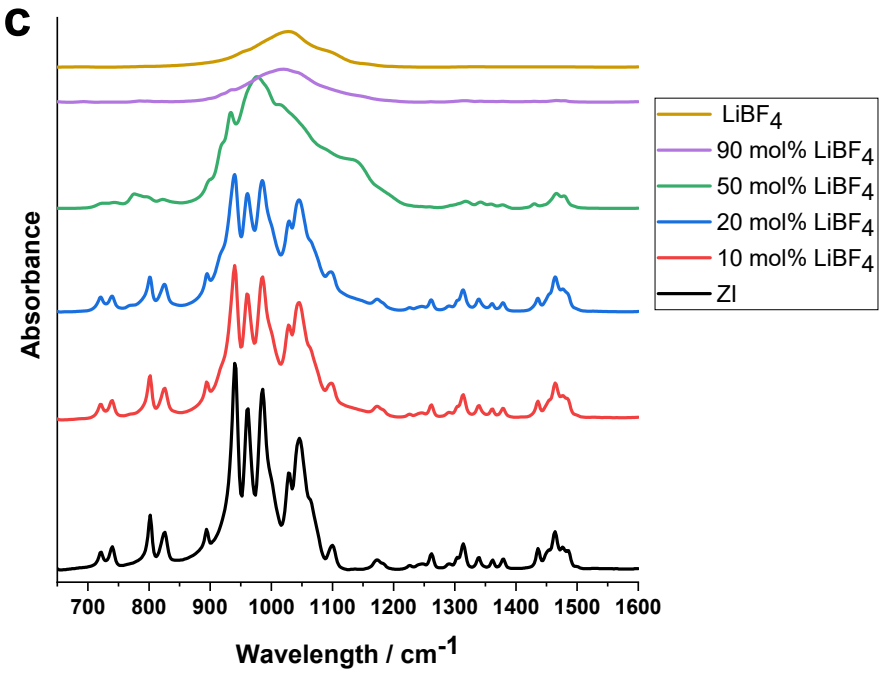

Figure S4. a) Comparison of the room temperature FTIR spectra of ZI, the ZI/10 mol% $LiBF_4$ and the ZI/10 mol% LiFSI. b) Comparison of the room temperature FTIR spectra of ZI and its mixture with LiFSI. c) Comparison of the room temperature FTIR spectra of ZI and its mixtures with $LiBF_4$

In general, the 10 and 20 mol% LiFSI in ZI spectra are relatively sharp and dominated by peaks from the ZI, whereas the 50 and 90% spectra are broader and dominated by the LiFSI signals. The 50% spectra shows the biggest change in peak position and relative peak intensities compared to the neat ZI or LiFSI, as discussed below. However, in both the LiFSI and $LiBF_4$ spectra many of the bands overlap forming very broad peaks that cannot be accurately deconvoluted.

*The FTIR spectra of the ZI/LiFSI electrolytes showed that the peaks do not experience significant changes at 10 and 20 mol% LiFSI, except for a new shoulder appearing at 920 cm^{-1} in 10 mol% LiFSI that increases in intensity in the 20 and 50 mol% LiFSI electrolyte. As a shoulder at this position also appears in the ZI/$LiBF_4$ spectra, this is tentatively concluded to be the result of a new Li-F interaction, where the F can be from the zwitterion or the salt. Some peaks related to the FSI group increased in intensity (*1380, 1362, 1218, 1181 cm^{-1}*) due to the increasing FSI concentration and also overlap with the ZI peaks occurring in those same regions.*

In the 50 mol% LiFSI in ZI electrolyte, the position of the alkyl group modes occurring at 1246, 1438, 1476 and 1464 cm^{-1} were not affected, but their relative intensity is lower compared to the lower LiFSI content samples. The peaks at 802, 1454 and 1484 cm^{-1} are no longer evident in the 50% sample. In addition, the ring modes shifted to lower wavenumber from 1045 cm^{-1} (ring breathing) in pure ZI to 1041 cm^{-1} in the 50% sample, and from 1028 ((Me–N), ($MeBF_3$–N) stretching) to 1024 cm^{-1}, with very low intensity. The shifts in the alkyl group and pyrrolidinium ring modes to the lower wavenumbers suggest weaker interactions between ZI and LiFSI, which is consistent with the liquid state of the sample. Similarly, the peaks located at 743, 837, 1147, 1359 and 1378 $cm^{-1}$are assigned to the FSI ion, which all occur at lower wavenumber compared to neat LiFSI.

The spectrum of the 90 mol% LiFSI sample shows the peaks related to the FSI anion at slightly lower wavenumber than in the other samples. The pyrrolidinium ring peaks occur at lower wavenumber with significant lower in intensity. Some alkyl peaks disappeared, due to the lower concentration of ZI, and some shifted to lower wavenumber. The observed shifts suggest the presence of a weaker interaction between LiFSI and ZI.

The spectrum of $LiBF_4$ in ZI (Figure S4c) indicate no significant effect of adding $LiBF_4$ up to 20 mol%, except for a slight shoulder appearing at 920 cm^{-1}. However, at 50 mol% $LiBF_4$, all alkyl modes (1045 and 1028 cm^{-1}) disappeared and the CH_3 and CH rocking shifts from 1099 in ZI to 1138 cm^{-1}. The alkyl modes at 1454 (CH_2 vibration), 1484 (CH_2 ring vibration) and 1246 cm^{-1} (CH_3CN-BF_3 stretching) disappeared, and the other alkyl peaks shifted to lower wavenumbers. The BF_4 peak at 1022 cm^{-1} in $LiBF_4$ shifted to lower wavenumbers of 978 cm^{-1}. Similar to the LiFSI mixtures, the shifting peaks to a lower wavenumbers and disappearance of some other peaks is consistent with the disordered, quasi-solid-state structure of 50 mol% $LiBF_4$ in ZI (as shown in the DSC data in Figure 2a). At the 90% $LiBF_4$ concentration, the spectra is very broad and essentially the same as for neat $LiBF_4$, with no distinguishable peaks from the ZI.

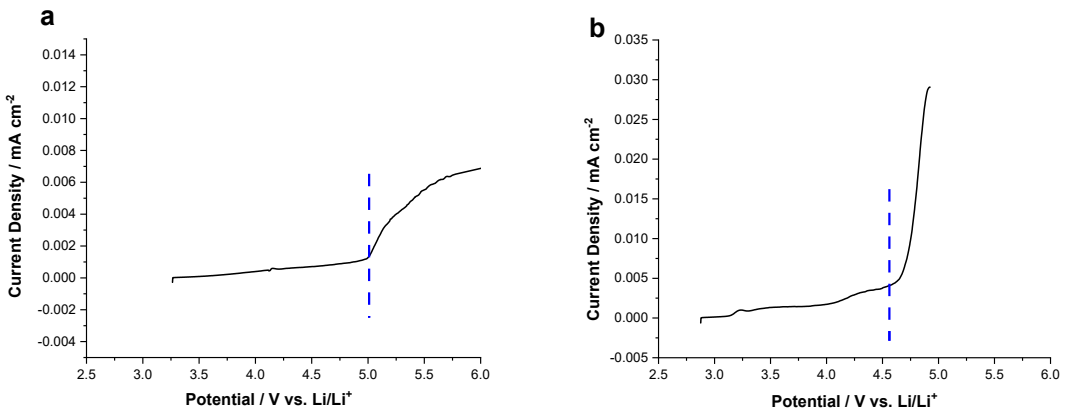

Figure S5. Linear sweep voltammograms obtained for the a) 50 mol% LiFSI b) 90 mol% LiFSI in ZI electrolyte at 50℃ collected at a scan rate of 0.05 mVs^{-1} using a stainless-steel working electrode versus a Li metal reference electrode.

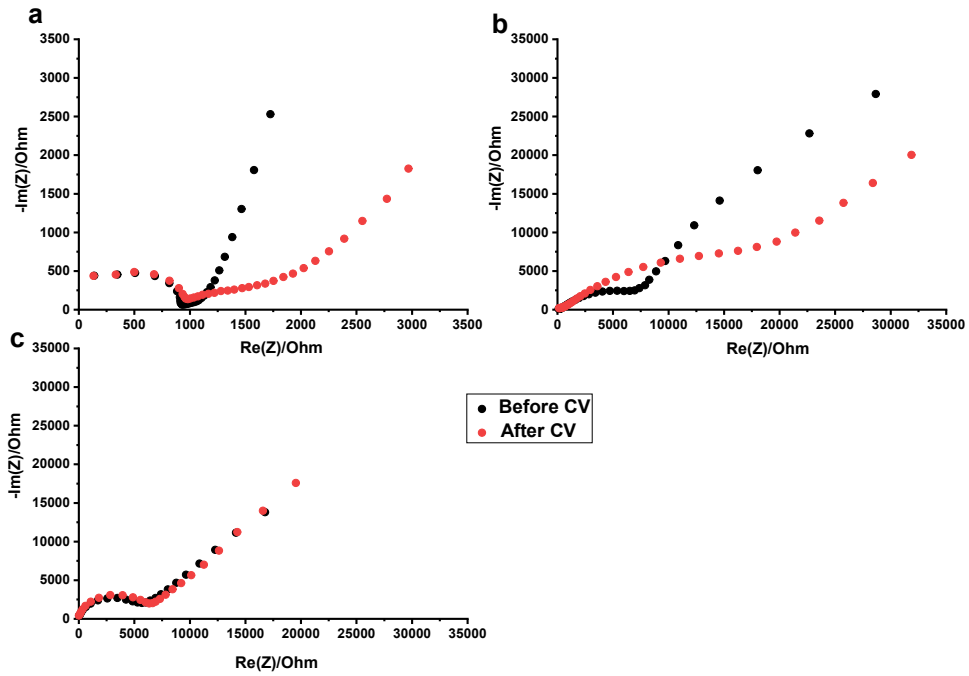

Figure S6. EIS data before and after CV scans of a) 90 mol% LiFSI, b) 90 mol% $LiBF_4$ and c) 10 mol% $LiBF_4$ in ZI.

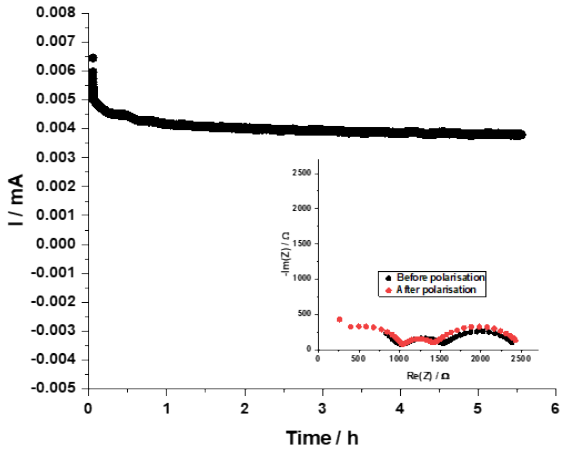

Figure S7. Li ion transference number of the 90 mol% LiFSI in ZI, measured using the Bruce-Vincent method based on constant voltage polarisation at 50 ℃. Inset - EIS plots before and after polarisation.

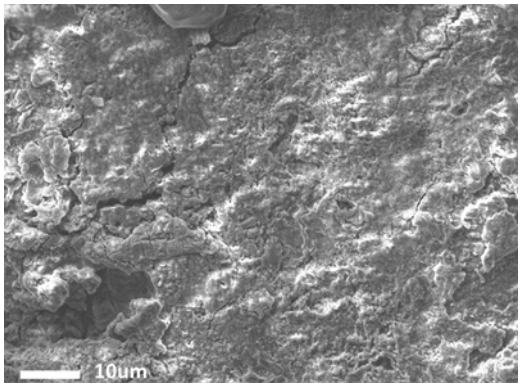

Figure S8. SEM image from the plated side of lithium metal symmetric cells after 1000 h of cycling

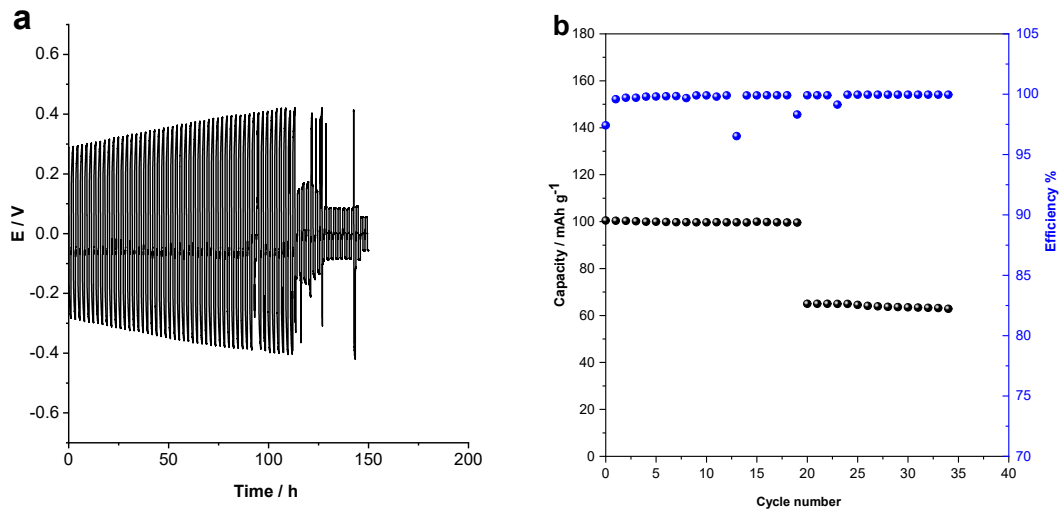

Figure S9. a) Potential (Ewe; V) vs. Time for the Li / 90 mol% LiFSI in [C_2mpyr][BF_4] / Li symmetric cell cycling at 0.1 mA cm^{-2} at 50 °C with charge and discharge intervals of 1 h. b) discharge capacity vs. cycle number for Li /LFP cells cycled at 50 °C

Table 1. Comparison of the ionic conductivity of the previously reported OIPCs.

OIPC	Li salt	mol%	Ionic conductivity / S cm^{-1}	Temperature / °C		Ref
[C_1mpyr][BF_4]	$LiBF_4$	5	5×10^{-7}	50	solid	1
[P_{1i444}FSI]FSI]	LiFSI	4	2.6×10^{-4}	22	solid	2
[C_2mpyr][FSI]	LiFSI	10	10^{-5}	50	solid	3
[C_2mpyr][FSI]	LiFSI	50	10^{-3}	50	liquid	4
[C_2mpyr][BF_4]	$LiBF_4$	10	4.2×10^{-8}	30	solid	5
[N_{1222}][TFSI]	LiTFSI	90	1×10^{-4}	50	solid	6
[N_{1222}][TFSI]	LiTFSI	10	8×10^{-3}	50	solid	6

$[N_{1222}][FSI]$	LiFSI	90	2×10^{-4}	50	solid	6
$[N_{1222}][FSI]$	LiFSI	10	5×10^{-2}	50	solid	6
[HMG][FSI]	LiFSI	10	6×10^{-4}	30	solid	7
[HMG][FSI]	LiFSI	90	5×10^{-4}	30	solid	
$[C_{(i3)}mpyr][FSI]$	LiFSI	50	1.5×10^{-3}	50	liquid	8
$[C_3mpyr][FSI]$	LiFSI	50	3×10^{-3}	50	liquid	
$[C_2epyr][FSI]$	LiFSI	50	2×10^{-3}	30	liquid	9
$[C_2epyr][FSI]$	LiFSI	90	2×10^{-4}	30	solid	

Table S2. Tentative Assignment of peaks in the IR Spectra of ZI, OIPC and the effect on the peak position upon adding 10 mol% LiBF4 and LiFSI.

	Peak position (cm^{-1})								
functional group	**ZI ($C_1mpyrBF_3$)**	**ZI/10 mol% $LiBF_4$**	**ZI/10 mol% LiFSI**	**OIPC $[C_2mpyr][BF_4]$**	**OIPC/10 mol% LiFSI**	**LiFSI**	**$LiBF_4$**	**Band assignment**	**Ref**
BF_4	740 1289 1002	740 1289 1000	740 1290 1000	- 1285 996	-	-	1022	vBF_4 vBF vBF	5
FSI	-	-	1380 1362 1218 1181	-	1382 1363 1217 1181 829 747	1370 1410 1210, 1144 1178, 1234 792, 810, 828, 868 756 856 896	-	$v_{as}SO_2$ $v_{as}SO_2$ v_sSO_2 v_sSO_2 vS-F v_sS-N-S $v_{as}S$-N-S $v_{ip}SF$	10
Pyrrolidinium ring	1045 1028	1045 1028	1045 1028	1045 1027	1047 1031			δ(ring) Ring breathing, v(Me–N), v ($MeBF_3$–N)	11
Alkyl groups	1099 1438 1454 1476 1484 802 1246 1464 - - -	1098 1438 1454 1476 1484 802 1246 1464 - - -	1099 1435 1454 1476 1484 802 1246 1464 - - -	1095 1436 1457 1471 - 810 - - 1406 1387 937	1095 1436 1456 1471 - 810 - - 1407 - 937			$\delta_{rock}(CH_3)+ \delta_{rock}$(C-H) $\delta_s(CH_3)_{Me}$ $\delta(CH_2)$ $\delta_{as}(CH_3)_{Me}$ $\delta(CH_2)$ (ring) γ(CH) vCH_3CN-BF_3 γCH_3 scissoring, out of phase $vs(CH_3)_{Et} + \delta_{wang}(CH_2)$ $vas(C\text{-}N)_{Et} + \delta_s(CH_3)_{Et}$ $v(C\text{-}C)_{Et}$	5 11 12

v_{as}: asymmetric stretch, v_s: symmetric stretch; δ_{as}: asymmetric deformation, δ_s : symmetric deformation, γ: out of plane deformation; ip: in-phase; Et: ethyl(—C_2H_5); Me : methyl(—CH_3).

References

1. L. Jin, P. Howlett, J. Efthimiadis, M. Kar, D. Macfarlane and M. Forsyth, *Journal of Materials Chemistry*, 2011, **21**, 10171-10178.
2. L. Jin, P. C. Howlett, J. M. Pringle, J. Janikowski, M. Armand, D. R. MacFarlane and M. Forsyth, *Energy & Environmental Science*, 2014, **7**, 3352-3361.
3. Y. Zhou, X. Wang, H. Zhu, M. Armand, M. Forsyth, G. W. Greene, J. M. Pringle and P. C. Howlett, *PCCP*, 2017, **19**, 2225-2234.
4. Y. Zhou, X. Wang, H. Zhu, M. Yoshizawa-Fujita, Y. Miyachi, M. Armand, M. Forsyth, G. W. Greene, J. M. Pringle and P. C. Howlett, *ChemSusChem*, 2017, **10**, 3135-3145.
5. N. Iranipour, D. J. Gunzelmann, A. Seeber, J. Vongsvivut, C. Doherty, F. Ponzio, L. A. O'Dell, A. F. Hollenkamp, M. Forsyth and P. C. Howlett, *Journal of Materials Chemistry A*, 2015, **3**, 6038-6052.
6. R. Yunis, D. Al-Masri, A. F. Hollenkamp, C. M. Doherty, H. Zhu and J. M. Pringle, *Journal of The Electrochemical Society*, 2020, **167**.
7. K. Biernacka, D. Al-Masri, R. Yunis, H. Zhu, A. F. Hollenkamp and J. M. Pringle, *Electrochimica Acta*, 2020, **357**, 136863.
8. D. Al-Masri, R. Yunis, A. F. Hollenkamp, C. M. Doherty and J. M. Pringle, *Physical Chemistry Chemical Physics*, 2020, **22**, 18102-18113.
9. D. Al-Masri, R. Yunis, H. Zhu, L. Jin, P. Bruce, A. F. Hollenkamp and J. M. Pringle, *Journal of Materials Chemistry A*, 2019, **7**, 25389-25398.
10. X. Li, Z. Zhang, S. Li, K. Yang and L. Yang, *Journal of Materials Chemistry A*, 2017, **5**, 21362-21369.
11. J. Adebahr, P. Johansson, P. Jacobsson, D. R. Macfarlane and M. Forsyth, *Electrochimica acta*, 2003, **48**, 2283-2289.
12. N. P. Wells and J. A. Phillips, *The Journal of Physical Chemistry A*, 2002, **106**, 1518-1523.